ECS Transactions, 50 (5) 137-144 (2012)
10.1149/05005.0137ecst ©The Electrochemical Society

The impact of oxide precipitates on minority carrier lifetime in Czochralski silicon

J.D. Murphy[a], K. Bothe[b], R. Krain[b], V.V. Voronkov[c], R.J. Falster[c,a]

[a] Department of Materials, University of Oxford, Parks Road, Oxford, OX1 3PH, UK
[b] Institut für Solarenergieforschung Hameln/Emmerthal, Am Ohrberg 1, 31860 Emmerthal, Germany
[c] MEMC Electronic Materials, via Nazionale 59, 39012 Merano, Italy

Oxide precipitates form in silicon for microelectronic and photovoltaic applications, and act as strong recombination centres. We have measured the injection-dependence of minority carrier lifetime in ~50 samples from p-type and n-type Czochralski silicon wafers with a wide range of precipitate densities. We find that all the data can be parameterized in terms of two independent Shockley-Read-Hall centres. The first is at $E_V + 0.22$eV, and has a capture coefficient for electrons 157 greater than that for holes. The second is at $E_C - 0.08$eV and has a capture coefficient for holes ~1,200 greater than that for electrons. The density of the centres is approximately dependent on the precipitate concentration. The existence of dislocations and stacking faults around the precipitates increases the density of both centres.

Introduction

Single-crystal Czochralski silicon (Cz-Si) is the substrate used for most microelectronic devices. Cast multi-crystalline silicon (mc-Si) and Cz-Si are also used for ~90% of photovoltaics (PV). Both materials have a high interstitial oxygen content (up to ~ 10^{18}cm^{-3}), usually arising from the dissolution of the melt-containing silica crucible. In Cz-Si for microelectronics, intentional high temperature annealing is often used to form oxide precipitates to act as sinks for mobile transition metal impurities as part of internal gettering processes [1, 2]. Unintentional oxide precipitation also occurs in the vacancy-rich material created by the fast production rates used for PV Cz-Si [3, 4] and in mc-Si upon ingot cooling [5-7]. The morphology of the precipitates evolves during growth from an unstrained to a strained state, and strained precipitates can be surrounded by dislocations and stacking faults [8, 9]. Oxide precipitates and surrounding defects are strong recombination centres [10-21] and hence can limit the conversion efficiency of silicon solar cells [4].

Minority carrier lifetime is an important figure of merit in semiconductor materials, particularly those used for PV. Shockley-Read-Hall (SRH) statistics are used to quantify recombination of charge carriers at many defects in semiconductors [22, 23]. The SRH parameters of a defect are its energy level in the bandgap and capture coefficients for electrons and holes. The approximate energy level and the ratio of the capture coefficient for electrons to that of holes can be determined using temperature- and injection-dependent lifetime spectroscopy (TIDLS) [24-26]. We have used TIDLS to parameterize recombination at oxide precipitates and surrounding defects in terms of SRH statistics [17, 19-21]. We review some of our results in this paper.

Experimental methods

Over 50 Cz-Si wafers were processed in very clean conditions to contain oxide precipitates, using conditions described in detail previously [17, 19]. P-type samples were doped with 3.9 x 10^{14} to 8.2 x 10^{15}cm^{-3} of boron; n-type samples were doped with 5 x 10^{13} to 1.0 x 10^{15}cm^{-3} of phosphorus. The strained precipitate density ($N_{strained}$) was measured by Schimmel etching and ranged from 3 x 10^{6} to 7 x 10^{10}cm^{-3}. The p-type samples were also characterized by transmission electron microscopy (TEM) and the results are discussed elsewhere [9]. The TEM investigation enabled the identification of samples in which some of the precipitates were surrounded by other extended defects (dislocations and stacking faults).

The surfaces of 5cm x 5cm samples were passivated using silicon nitride grown by plasma enhanced chemical vapour deposition. Most samples were passivated using a remote plasma system, which has been shown to give surface recombination velocities below 10cm/s [27]. Minority carrier lifetime measurements were made using transient and quasi-steady-state photoconductance methods [28], using Sinton lifetime testers. The set-up used for temperature-dependent measurements is described elsewhere [26]. Immediately prior to measurement, samples were subjected to a 10 minute anneal at 200°C to dissociate boron-oxygen defects [29] and multiple close-up flashes of light to dissociate FeB pairs [30]. A subsequent measurement more than 24 hours later allows the bulk iron concentration to be determined using methods described previously [17, 31]. The bulk iron concentration in each sample was < 4 x 10^{11}cm^{-3} [17].

Analysis of lifetime data

The measured minority carrier lifetime, τ_{measured}, includes contributions from processes other than recombination at oxide precipitates and surrounding defects. We present our data in terms of a residual lifetime defined according to:

$$\frac{1}{\tau_{\text{residual}}} = \frac{1}{\tau_{\text{measured}}} - \left(\frac{1}{\tau_{\text{band-to-band}}} + \frac{1}{\tau_{\text{CE Auger}}} + \frac{1}{\tau_{\text{Fe}_i}} \right) \quad (1)$$

where $\tau_{\text{band-to-band}}$ is the lifetime due to band-to-band recombination [32], $\tau_{\text{CE Auger}}$ is the lifetime due to Coloumb-enhanced Auger recombination [33] and τ_{Fe_i} is the lifetime due to SRH recombination at bulk interstitial iron [34]. Details of these corrections are given in our previous paper [17]. In n-type silicon it is not possible to measure the interstitial iron concentration, so no correction is made for bulk iron-related recombination in n-type samples. For samples with low precipitate densities (high measured lifetimes) the corrections can be significant, particularly at high injection where Coulomb-enhanced Auger recombination is non-negligible.

To analyse our data we use a linear formulation of SRH statistics, which has been discussed in detail elsewhere [19]. In p-type material the electron lifetime is expressed as a linear function of $X = n/p$, where n is the total electron concentration and p is the total hole concentration, according to:

$$\tau_n = \frac{1}{\alpha_n N}\left[1 + \frac{Qn_1}{p_0} + \frac{p_1}{p_0} + X\left(Q - \frac{Qn_1}{p_0} - \frac{p_1}{p_0}\right)\right] \quad (2)$$

where α_n is the defect's capture coefficient for electrons, N is the defect concentration, $Q = \alpha_n / \alpha_p$ where α_p is the defect's capture coefficient for holes, and p_0 is the equilibrium hole concentration. The SRH densities are given by $n_1 = N_C \exp\left(-\frac{(E_C - E_T)}{kT}\right)$ and $p_1 = N_V \exp\left(-\frac{(E_T - E_V)}{kT}\right)$, where N_C is the density of states in the conduction band, N_V is the density of states in the valence band, and E_T is the energy level of the defect.

In n-type material the hole lifetime is expressed as a linear function of $Y = p/n$ according to:

$$\tau_p = \frac{1}{\alpha_p N}\left[1 + \frac{n_1}{n_0} + \frac{p_1}{n_0 Q} + Y\left(\frac{1}{Q} - \frac{n_1}{n_0} - \frac{p_1}{Qn_0}\right)\right] \quad (3)$$

where n_0 is the equilibrium electron concentration.

The lifetime corresponding to a single-level defect appears as a linear function of X (for p-type) of Y (for n-type) in this framework of SRH statistics. If more than one single-level defect operates independently, lifetimes can be added in reciprocal. It is therefore straightforward to separate the effects of multiple independent defects using this approach.

Results and analysis

Figure 1 shows the residual minority carrier lifetime versus *n/p* for two p-type samples measured at room temperature. Dislocations and stacking faults were found to surround the oxide precipitates for one sample, but not the other. Very similar injection-dependence was seen in all other p-type samples studied [17, 19]. Figure 2 shows the residual minority carrier lifetime versus *p/n* for n-type samples with different doping levels. Figure 3 shows the residual lifetime measured at selected temperatures in a p-type and an n-type sample. The lifetime increases with increasing temperature in both cases.

In our recent publication [19] we have shown how injection-dependent lifetime data can be analysed in terms of SRH statistics, using oxide precipitates as a case study. Our approach is to fit the data with independent defects according to Equation 2 (for p-type) or Equation 3 (for n-type). For all conditions investigated, we find that the injection-dependent lifetime data can be fitted using just two independent centres. We refer to these as "Defect 1" and "Defect 2". By analyzing samples with different doping levels we are able to determine the values of Q for each defect and the energy levels of the defects. We find that Defect 1 has Q_1 = 157 and lies at E_V + 0.22eV. We find that Defect 2 has $1/Q_2$ = 1,200 and lies at E_C – 0.08eV. The temperature-dependent data show that the capture coefficient for holes at Defect 1 (α_{p1}) decreases with temperature with a 0.20eV activation energy, and that the capture coefficient for electrons at Defect 2 (α_{n2}) decreases with temperature with a 0.14eV activation energy.

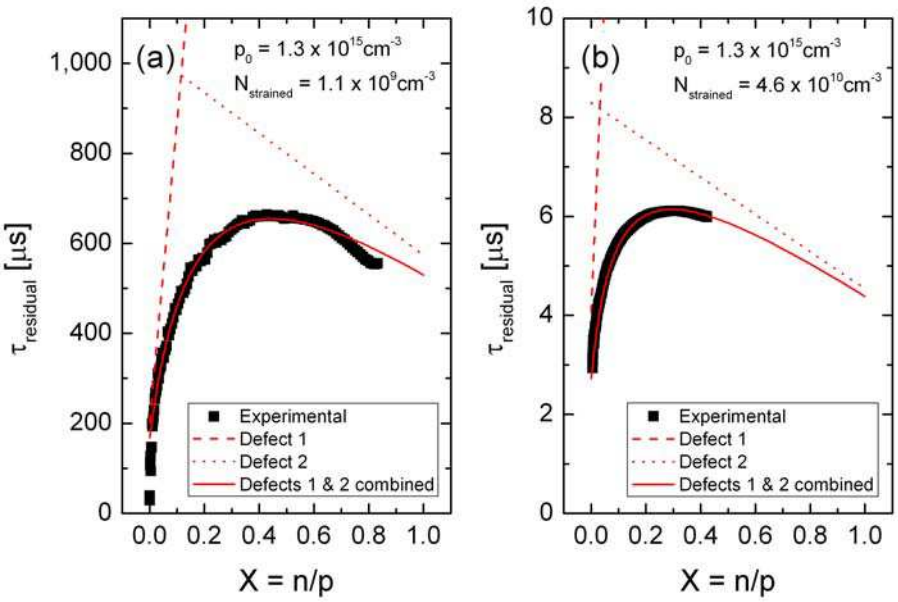

Figure 1. Residual minority carrier lifetime versus *n/p* for two typical p-type samples at room temperature. Graph (a) is for a sample processed with an 8h nucleation and 2h growth to contain oxide precipitates not surrounded by other extended defects such as dislocations and stacking faults. Graph (b) is for a sample processed with a 32h nucleation and an 8h growth to contain oxide precipitates surrounded by dislocations and stacking faults.

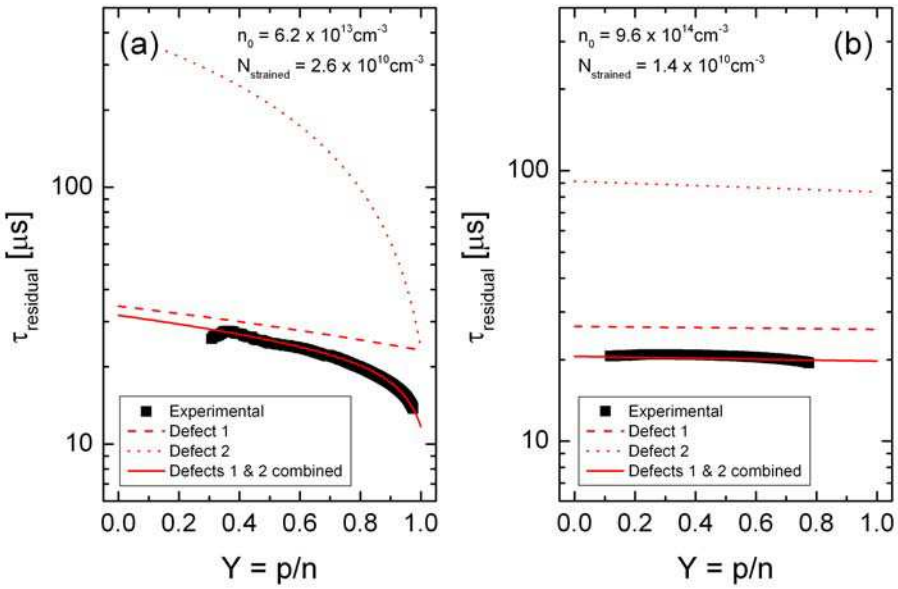

Figure 2. Residual minority carrier lifetime versus *p/n* for two typical n-type samples at room temperature.

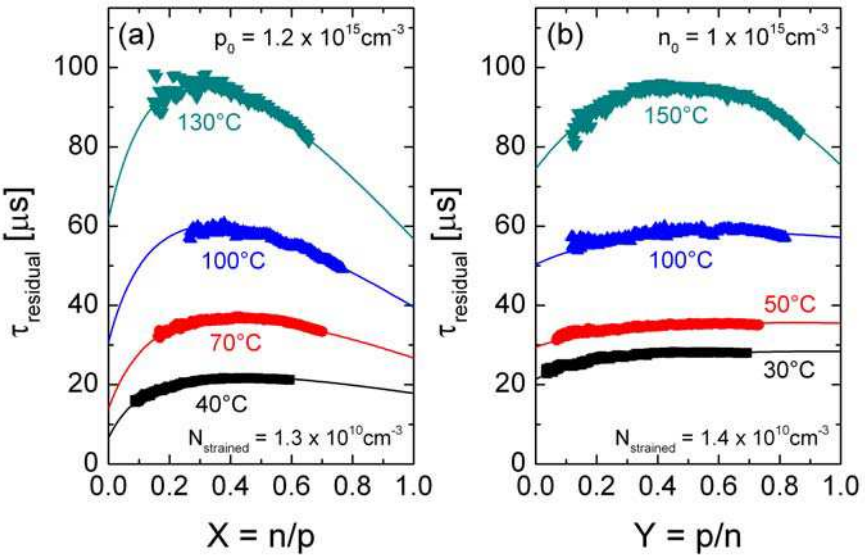

Figure 3. Residual minority carrier lifetime at different measurement temperatures plotted against (a) *n/p* for a p-type sample and (b) *p/n* for an n-type sample. The experimental data have been fitted using two independent SRH centres.

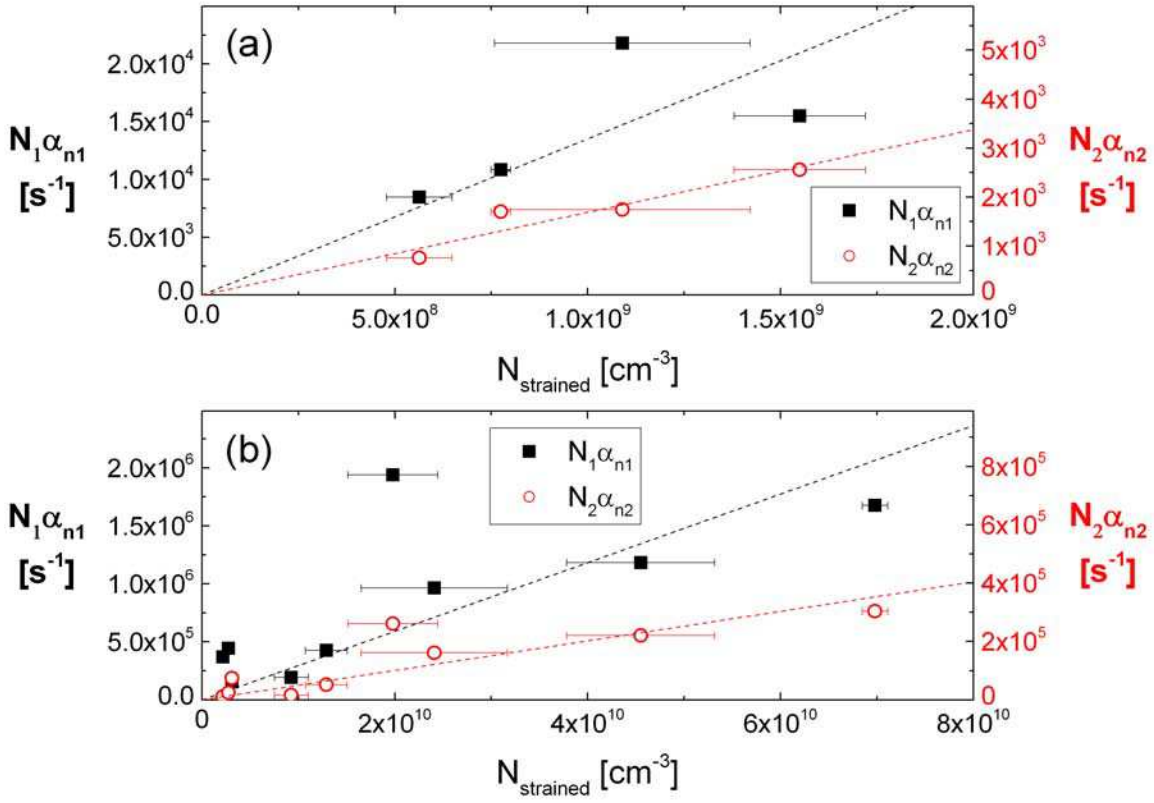

Figure 4. Variation in the $N_1\alpha_{n1}$ and $N_2\alpha_{n2}$ fit parameters versus density of strained precipitates in p-type silicon. In Graph (a) the oxide precipitates were not surrounded by dislocations and stacking faults; in Graph (b) dislocations and stacking faults were found to surround some of the oxide precipitates.

The injection-dependent lifetime data can also be analysed to give information on the density of the two independent SRH centres. For example, in the p-type case, extrapolation of Equation 2 to the $X \rightarrow 0$ limit enables $\alpha_n N$ to be found when the SRH parameters are pre-determined. Although it is not possible to separate the state density from the capture coefficient, if the capture coefficient does not vary, the relative state density between specimens can be determined. Figure 4 shows the variation of the $\alpha_n N$ parameter with the density of strained precipitates for p-type samples in which oxide precipitates are: (a) not surrounded by dislocations and stacking faults; and (b) surrounded by dislocations and stacking faults. The subscripts indicate whether the parameter is for Defect 1 or Defect 2. In both plots, the correlation of $N_1\alpha_{n1}$ and $N_2\alpha_{n2}$ with $N_{strained}$ is approximately linear. The gradients of the best-fit lines constrained to pass through the origin are: (a) 1.7 x 10^{-5}cm^{3}s^{-1} for $N_1\alpha_{n1}$ and 1.8 x 10^{-6}cm^{3}s^{-1} for $N_2\alpha_{n2}$ for samples in which oxide precipitates are not surrounded by other extended defects; and (b) 2.9 x 10^{-5}cm^{3}s^{-1} for $N_1\alpha_{n1}$ and 5.1 x 10^{-6}cm^{3}s^{-1} for $N_2\alpha_{n2}$ for samples in which dislocations or stacking faults were found to surround some of the oxide precipitates.

Discussion

From our analysis of injection-dependent lifetime data we have shown that recombination at oxide precipitates can be parameterised in terms of two independent defects. We have provided an empirical relation between the precipitate density and the recombination activity. Although the uncertainties in this are significant (a factor of two at best in the case of the dislocation-free precipitates), this parameterisation can be used to quantify the effect of oxide precipitates on minority carrier lifetime in silicon. This is important as it means a relatively straightforward etching experiment can be used to place an upper limit on the minority carrier lifetime of the material.

By correlating the lifetime measurements with TEM analysis, the effect of the surrounding extended defects (dislocations and stacking faults) has been studied. It is notable that no additional states are required to fit the injection-dependent lifetime curves in the presence of surrounding defects (Figure 1). Figure 4 shows the relationship between $N_1\alpha_{n1}$ and $N_2\alpha_{n2}$ and precipitate density. The fact that this linear relationship is only approximate is not surprising given the large differences in structure between precipitates and surrounding defects that can occur. Figure 4 shows that $N_1\alpha_{n1}$ is an average factor of ~1.7 higher per precipitate and $N_2\alpha_{n2}$ is an average factor of ~2.9 higher per precipitate than for the samples in which no dislocations or stacking faults were found to surround the precipitates. Thus, it appears that other extended defects around the precipitates give rise to more of the same recombination-active defects that are associated with just the precipitates themselves.

Oxide precipitates and associated dislocations and stacking faults are well-known to act as gettering centres for metallic impurities [1, 2]. Even though the samples studied were processed in ultra-clean conditions, bulk iron concentrations of up to 4 x 10^{11}cm^{-3} were measured in the p-type samples [17]. Low levels of impurity contamination are known strongly to affect the recombination properties of extended defects in silicon [35, 36]. The fact that the presence of dislocations and stacking faults increase the density of the *same* recombination centres could mean that at least some of the recombination activity is impurity-related. This is the subject of further investigation.

Conclusions

Oxide precipitates are important defects in silicon for microelectronics and PV. To quantify their effect on minority carrier lifetime we have performed measurements on samples with different types, resistivities and concentrations of strained precipitates. For most practical purposes in photovoltaics (*i.e.* low temperatures and moderate doping) the lifetime data can be parameterised in terms of just two independent defects. Defect 1 has a single energy level at E_V + 0.22eV and has a capture coefficient for electrons ~157 times greater than its capture coefficient for holes at room temperature. The capture coefficient for holes at Defect 1 decreases with temperature with a 0.20eV activation energy. Defect 2 has a single energy level at E_C – 0.08eV and has a capture coefficient for holes ~1,200 times greater than its capture coefficient for electrons at room temperature. The capture coefficient for electrons at Defect 2 decreases with temperature with a 0.14eV activation energy. Dislocations and stacking faults around the oxide precipitates increase the concentrations of the two defects, without introducing additional states into the bandgap. The role of impurities segregated to the oxide precipitates and surrounding defects requires further investigation.

Acknowledgments

The authors are very grateful to D. Gambaro, M. Olmo and M. Cornara at MEMC for performing the thermal treatments and precipitate density measurements, to staff at ISFH for surface passivation by remote PECVD, to R. Chakalova at Oxford for surface passivation by direct PECVD, and to V.Y. Resnik at the Institute of Rare Metals (Moscow) for performing TEM analysis. J.D.M. is the holder of a Royal Academy of Engineering/ EPSRC Research Fellowship. Funding from a Research Grant from the Royal Society and an EPSRC First Grant is also gratefully acknowledged.

References

1. R. J. Falster and W. Bergholz, *Journal of the Electrochemical Society* **137**, 1548 (1990).
2. D. Gilles, E. R. Weber and S. Hahn, *Physical Review Letters* **64**, 196 (1990).
3. P. K. Kulshreshtha, Y. Yoon, K. M. Youssef, E. A. Good and G. Rozgonyi, *Journal of the Electrochemical Society* **159**, H125 (2012).
4. J. Haunschild, I. E. Reis, J. Geilker and S. Rein, *Physica Status Solidi Rapid Research Letters* **5**, 199 (2011).
5. H. J. Möller, C. Funke, A. Lawerenz, S. Riedel and M. Werner, *Solar Energy Materials & Solar Cells* **72**, 403 (2002).
6. M. Tajima, Y. Iwata, F. Okayama, H. Toyota, H. Onodera and T. Sekiguchi, *Journal of Applied Physics* **111**, 113523 (2012).
7. K. Bothe, K. Ramspeck, D. Hinken, C. Schinke, J. Schmidt, S. Herlufsen, R. Brendel, J. Bauer, J.-M. Wagner, N. Zakharov and O. Breitenstein, *Journal of Applied Physics* **106**, 104510 (2009).
8. W. Bergholz, M. J. Binns, G. R. Booker, J. C. Hutchison, S. H. Kinder, S. Messoloras, R. C. Newman, R. J. Stewart and J. G. Wilkes, *Philosophical Magazine B* **59**, 499 (1989).

9. R. Falster, V. V. Voronkov, V. Y. Resnik and M. G. Milvidskii, in *Proceedings of the Electrochemical Society, High Purity Silicon VIII* (2004), Vol. 200405, pp. 188.
10. K. H. Yang, H. F. Kappert and G. H. Schwuttke, *Physica Status Solidi A* **50**, 221 (1978).
11. M. Miyagi, K. Wada, J. Osaka and N. Inoue, *Applied Physics Letters* **40**, 719 (1982).
12. S. S. Chan, C. J. Varker, J. D. Whitfield and R. W. Carpenter, *Materials Research Society Symposium Proceedings* **46**, 281 (1985).
13. J. M. Hwang and D. K. Schroder, *Journal of Applied Physics* **59**, 2476 (1986).
14. J. Vanhellemont, E. Simoen, A. Kaniava, M. Libezny and C. Claeys, *Journal of Applied Physics* **77**, 5669 (1995).
15. W. Seifert, M. Kittler and J. Vanhellemont, *Materials Science and Engineering B* **42**, 260 (1996).
16. T. Mchedlidze, K. Matsumoto and E. Asano, *Japanese Journal of Applied Physics* **38**, 3426 (1999).
17. J. D. Murphy, K. Bothe, M. Olmo, V. V. Voronkov and R. J. Falster, *Journal of Applied Physics* **110**, 053713 (2011).
18. V. Lang, J. D. Murphy, R. J. Falster and J. J. L. Morton, *Journal of Applied Physics* **111**, 013710 (2012).
19. J. D. Murphy, K. Bothe, R. Krain, V. V. Voronkov and R. J. Falster, *Journal of Applied Physics* **111**, 113709 (2012).
20. J. D. Murphy, K. Bothe, M. Olmo, V. V. Voronkov and R. J. Falster, *ECS Transactions* **33**, 121 (2010).
21. J. D. Murphy, K. Bothe, R. Krain, M. Olmo, V. V. Voronkov and R. J. Falster, *Solid State Phenomena* **178-179**, 205 (2011).
22. R. N. Hall, *Physical Review* **87**, 387 (1952).
23. W. Shockley and W. T. Read, *Physical Review* **87**, 835 (1952).
24. S. Rein, T. Rehrl, W. Warta and S. W. Glunz, *Journal of Applied Physics* **91**, 2059 (2002).
25. D. Macdonald and A. Cuevas, *Physical Review B* **67**, 075203 (2003).
26. J. Schmidt, *Applied Physics Letters* **82**, 2178 (2003).
27. T. Lauinger, J. Moschner, A. G. Aberle and R. Hezel, *Journal of Vacuum Science & Technology B* **16**, 530 (1998).
28. R. A. Sinton and A. Cuevas, *Applied Physics Letters* **69**, 2510 (1996).
29. K. Bothe and J. Schmidt, *Journal of Applied Physics* **99**, 013701 (2006).
30. G. Zoth and W. Bergholz, *Journal of Applied Physics* **67**, 6764 (1990).
31. J. D. Murphy and R. J. Falster, *Physica Status Solidi Rapid Research Letters* **5**, 370 (2011).
32. H. Schlangenotto, H. Maeder and W. Gerlach, *Physica Status Solidi A* **21**, 357 (1974).
33. M. J. Kerr and A. Cuevas, *Journal of Applied Physics* **91**, 2473 (2002).
34. S. Rein and S. W. Glunz, *Journal of Applied Physics* **98**, 113711 (2005).
35. V. Kveder, M. Kittler and W. Schröter, *Physical Review B* **63**, 115208 (2001).
36. T. S. Fell, P. R. Wilshaw and M. D. de Coteau, *Physica Status Solidi A* **138**, 695 (1993).